Contaminant transport in a fracture with spatially variable aperture in the presence of monodisperse and polydisperse colloids

ARTICLE *in* STOCHASTIC ENVIRONMENTAL RESEARCH AND RISK ASSESSMENT · SEPTEMBER 2005

Impact Factor: 2.67 · DOI: 10.1007/s00477-004-0231-3

3 AUTHORS, INCLUDING:

Scott C James
Baylor University
118 PUBLICATIONS **579** CITATIONS

SEE PROFILE

Constantinos V. Chrysikopoulos
Technical University of Crete
143 PUBLICATIONS **1,990** CITATIONS

SEE PROFILE

Stoch Environ Res Risk Assess (2005) 19: 266–279
DOI 10.1007/s00477-004-0231-3

ORIGINAL PAPER

Scott C. James · Tanya K. Bilezikjian
Constantinos V. Chrysikopoulos

Contaminant transport in a fracture with spatially variable aperture in the presence of monodisperse and polydisperse colloids

Published online: 12 February 2005

Abstract A quasi-three-dimensional particle tracking model is developed to characterize the spatial and temporal effects of advection, molecular diffusion, Taylor dispersion, fracture wall deposition, matrix diffusion, and co-transport processes on two discrete plumes (suspended monodisperse or polydisperse colloids and dissolved contaminants) flowing through a variable aperture fracture situated in a porous medium. Contaminants travel by advection and diffusion and may sorb onto fracture walls and colloid particles, as well as diffuse into and sorb onto the surrounding porous rock matrix. A kinetic isotherm describes contaminant sorption onto colloids and sorbed contaminants assume the unique transport properties of colloids. Sorption of the contaminants that have diffused into the matrix is governed by a first-order kinetic reaction. Colloids travel by advection and diffusion and may attach onto fracture walls; however, they do not penetrate the rock matrix. A probabilistic form of the Boltzmann law describes filtration of both colloids and contaminants on fracture walls. Ensemble-averaged breakthrough curves of many fracture realizations are used to compare arrival times of colloid and contaminant plumes at the fracture outlet. Results show that the presence of colloids enhances contaminant transport (decreased residence times) while matrix diffusion and sorption onto fracture walls retard the transport of contaminants. Model simulations with the polydisperse colloids show increased effects of co-transport processes.

S. C. James (✉)
Geohydrology Department, Sandia National Laboratories,
Albuquerque, NM 87185 0735, USA
E-mail: scjames@sandia.gov

T. K. Bilezikjian
RBF Consulting, 14725 Alton Parkway, Irvine,
CA 92618, USA
E-mail: tanyab@rbf.com

C. V. Chrysikopoulos
Department of Civil Engineering,
University of Patras, Rio, 26500, Greece
E-mail: gios@upatras.gr

Keywords Colloid and contaminant co-transport · Particle tracking · Variable aperture fracture

Nomenclature

b	Uniform fracture aperture, L
$\bar{b}$	Mean aperture of the variable aperture fractures, L
$b(x,y)$	Local fracture aperture, L
C_f	Number of aqueous contaminants in an element
C^*_f	Number of contaminants in an element sorbed onto colloids
d_p	Colloid diameter, L
$\mathcal{D}_\mathrm{n}$	Molecular diffusion coefficient for a colloid, L^2/t
$\mathcal{D}_\mathrm{c}$	Molecular diffusion coefficient for a contaminant, L^2/t
D_eff	Effective dispersion coefficient for the colloid plume, L^2/t
D_Taylor	Taylor dispersion coefficient for a contaminant plume, L^2/t
j	Element number of a variable aperture fracture in the y-direction
k	Boltzmann's constant, $\mathrm{ML}^2/\mathrm{Tt}^{\,2}$
k_f	Forward sorption rate of contaminants onto the matrix, 1/t
k_r	Reverse sorption rate for contaminants from the matrix, 1/t
K_n	Contaminant partition coefficient to aqueous colloids, L/t
K^*_n	Contaminant partition coefficient to deposited colloids, L/t
K_r	Reversible sorption rate for a contaminant on a colloid, 1/t
m	Step number in the particle tracking equation
$\bar{n}$	Colloid number concentration averaged across the uniform aperture fracture, $1/\mathrm{L}^3$
n_0	Initial number concentration of colloids or contaminants, $1/\mathrm{L}^3$
p_a	Probability of colloid or contaminant attachment per wall encounter

p_c	Probability of contaminant encountering the fracture wall in a time step
Re	Reynolds number, equal to $\rho\bar{u}_x b/\mu$.
Rn(0,1)	Uniformly distributed random number between 0 and 1
t	Time, t
t_e	Time for an expected 0.5 probability of a wall collision for a contaminant, t
t_f	Time after matrix penetration until a contaminant sorbs, t
t_r	Contaminant sorption time on the matrix, t
$t_{\Delta-e}$	Remaining portion of a time step once a contaminant has diffused into the matrix, t
Δt	Time step for the particle tracking algorithm, t
T	Absolute temperature of the interstitial fluid, T
u_x	Local Poiseuille fluid velocity in the x-direction, L/t
$\bar{u}_x$	Mean fluid velocity in the x-direction, L/t
u_y	Local fluid velocity in the y-direction, variable aperture fracture, L/t
$\bar{u}_y$	Mean fluid velocity in the y-direction, variable aperture fracture, L/t
$U_{\mathcal{D}}$	Deterministic velocity due to a diffusivity gradient, L/t
U_{eff}	Effective velocity of the colloid plume, L/t
U_θ	Deterministic velocity due to a porosity gradient, L/t
x	Coordinate along the fracture length, L
y	Coordinate along the fracture width, L
z	Coordinate normal to the fracture surface, L
z_{matrix}	Contaminant's z-location when diffused within matrix, L
$Z(0,1)$	A standard normally distributed random number

Greek Letters

θ	Matrix porosity
μ	Fluid dynamic viscosity, M/Lt
μ_{d_p}	Mean colloid diameter of a polydisperse plume, L
ρ	Density of the interstitial fluid, M/L^3
σ_{d_p}	Standard deviation of colloid diameter for a polydisperse plume, L
$\sigma^2_{\ln\, b}$	Variance of the log aperture fluctuations
Φ_c	Interaction energy between contaminants and the fracture wall, ML^2/t^3
Φ_n	Interaction energy between colloids and the fracture wall, ML^2/t^3

Introduction

Colloid facilitated contaminant transport has received considerable attention because radioactive wastes are stored in subsurface repositories. Although low permeability rock media and salt formations are good candidates for waste sequestration sites, the presence of fractures and colloids in a saturated environment may provide a mechanism for enhanced transport of escaped radionuclides and other low solubility, aqueous phase contaminants.

Experimental and field studies indicate that contaminants can migrate not only as dissolved species in the liquid phase, but also when adsorbed onto suspended colloidal particles (Champ and Schroeter 1988; Toran and Palumbo 1992; Hinsby et al. 1996; Vilks et al. 1996; Pang and Close 1999; Vilks and Baik 2001). For example, at the Nevada Test Site, radionuclide analyses for detonation cavity samples indicated that substantial fractions of selected nuclides are associated with natural clay, zeolite, and cristobalite colloids (Kersting et al. 1999). Colloids may serve as carriers for contaminants and significantly influence the net rate of contaminant migration (Mckay et al. 1993). At two separate sites at Los Alamos, New Mexico, plutonium and americium were detected at much greater distances from the source than predicted by dual porosity transport models (Nelson and Orlandini 1986). These findings compelled researchers to develop transport models that account for colloid-facilitated contaminant transport. These models suggest that depending on system conditions, the presence of colloids in a single fracture may either enhance or retard contaminant transport (e.g., Grindrod 1993; Smith and Degueldre 1993; Abdel-Salam and Chrysikopoulos 1995a, b; Ibaraki and Sudicky 1995a, b; Baek and Pitt 1996; Cvetkovic 2000; Marseguerra et al. 2001a, b; Bekhit and Hassan 2005).

Colloids are present in the subsurface in the form of metal oxides, humic macromolecules, bacteria, and viruses (van de Ven 1989). In fractured media, colloids are often formed by microerosion of minerals present in the subsurface environment as a result of formation crushing in association with tectonic activity (Drever 1985). Colloids are very fine particles that range in diameter between 10^{-3} μm and 10 μm (Stumm 1977), often with behaviors described by the well established DLVO theory (Derjaguin 1934; Verwey and Overbeek 1948). Because colloids have a high surface area per unit mass, they provide contaminants with the opportunity to migrate while sorbed onto their surface (Ouyang et al. 1996). Colloids also transport differently from solutes (Sirivithayapakorn and Keller 2003; Auset and Keller 2004; Keller et al. 2004).

In this paper, the paths of colloids and contaminants in a water-saturated fracture are tracked for many different realizations of a stochastically-generated, three-dimensional, variable aperture fracture. Both monodisperse and polydisperse colloid distributions are considered. Individual elution times for each colloid and contaminant from each fracture realization are incorporated into cumulative normalized ensemble average breakthrough curves. By comparing the characteristics of these curves for varied model parameters (e.g., dispersion and retardation), the individual and combined effects of various transport mechanisms and model

parameters on particle transport behavior are observed. Ultimately, the shapes of breakthrough curves incorporating all of the transport mechanisms—diffusion, sorption, and co-transport—are compared and contrasted.

While numerous parameter and discretization modifications could be applied to this work to more closely approximate a natural site, for example the colloid and contaminant retardation experiments of Grimsel (Smith et al. 2001), the purpose of this research is to demonstrate the utility of particle tracking modeling when applied to colloid and contaminant co-transport. Although reasonable parameter values have been employed for the model simulations presented in this work, no attempt was made to match them to a particular field site. Furthermore, because of the relatively large number of variables associated with colloid and contaminant co-transport, only the most important and controlling parameters are investigated.

Fracture description

Figure 1 is a simplified illustration of the general system modeled in this work. The quasi-three-dimensional fracture used in this study is 8 m long (x-direction) and 4 m wide (y-direction). The fracture plane is partitioned into 12,800 discrete square elements such that each 5×5 cm^2 element exhibits a distinct aperture. The size and discretization of the fracture were chosen for numerical convenience; any size fracture and corresponding elements could be selected given sufficient computational resources. The aperture field is generated stochastically with the geostatistical code SPRT2D (Gutjahr 1989). It is assumed that the aperture distribution in the fracture plane follows a log-normal distribution (Johns et al. 1993; Reimus et al. 1993; Keller 1998) with preselected mean and variance. Furthermore, the aperture distribution is assumed to vary spatially according to an isotropic exponential autocovariance function with specified correlation length (Chrysikopoulos and Abdel-Salam 1997). In this work, the average aperture of each fracture is $\bar{b} = 5 \times 10^{-5}$ m, the variance of the log-transformed aperture field is $\sigma^2_{\ln b} = 0.15$, and the isotropic correlation length is 1 m. Unique realizations of the aperture field are obtained by changing the seed number of the random field generator. The effects of fracture aperture anisotropy on colloid transport without contaminants have been examined (Chrysikopoulos and James 2003), consequently only the ideal case of an isotropic aperture field will be investigated here.

A fully implicit finite difference technique is used to calculate the pressure within each fracture element by solving the Reynolds lubrication equation (Abdel-Salam and Chrysikopoulos 1995b; James and Chrysikopoulos 2000; Chrysikopoulos and James 2003). Average velocity components in the x- and y-directions are then calculated for every element using steady-state volumetric fluxes. The Reynolds numbers in this work are well within the laminar range, Re$\sim 2.3\times10^{-3}$. Because the fluid flow is laminar and the no-slip condition is applied at the fracture walls, a parabolic velocity profile exists within each element. The parabolic velocities in the x- and y-directions are expressed in terms of these average velocities as

$$u_x(x,y,z) = \bar{u}_x(x,y)\frac{3}{2}\left\{1 - 4\left[\frac{z}{b(x,y)}\right]^2\right\}, \quad (1)$$

$$u_y(x,y,z) = \bar{u}_y(x,y)\frac{3}{2}\left\{1 - 4\left[\frac{z}{b(x,y)}\right]^2\right\}, \quad (2)$$

where $\bar{u}_x$ and $\bar{u}_y$ are the average fluid velocities in the x- and y-directions, respectively. There is no advective component in the z-direction, normal to the fracture surface and $z = 0$ at the center of the fracture and $\pm b(x,y)/2$ at the walls.

Zero fluxes at the upper and lower bounds ($y = 0$ m and $y = 4$ m) of the fracture ensure that all mass that enters the system at $x = 0$ m exits at $x = 8$ m. Thus, colloids and contaminants may enter only at the left hand (upstream) boundary of the system, and exit at the right hand (downstream) boundary. Attachment and sorption processes, however, allow colloids and contaminants to remain within the system.

One hundred fracture realizations and 10,000 particles per plume are used so that random noise, everpresent in stochastic simulations, is smoothed out through the averaging process. Ensemble averages of the resulting colloid and contaminant elution times yield cumulative normalized breakthrough curves.

Numerical model

Particle tracking

A particle tracking algorithm is used to track the movement of each colloid and contaminant in the system. The position and status (in suspension, attached onto surfaces, etc.) of each particle is updated every time step. Particle tracking techniques used with an appropriate time step yield excellent solutions to the advection-diffusion equation, provided that a sufficient number of particles are used in each simulation (Hassan and Mohamed 2003).

The numerical model used in this study is 3D for colloids, and 2D for contaminants within the fracture. It will be shown that computational restrictions on the time step prevent the contaminants from being tracked in the z-direction within the fracture because the diffusion distance for even a relatively small time step often results in contaminants moving irretrievably far into the fracture matrix. Nevertheless, as discussed in a subsequent section, this limitation does not compromise the accuracy of the model.

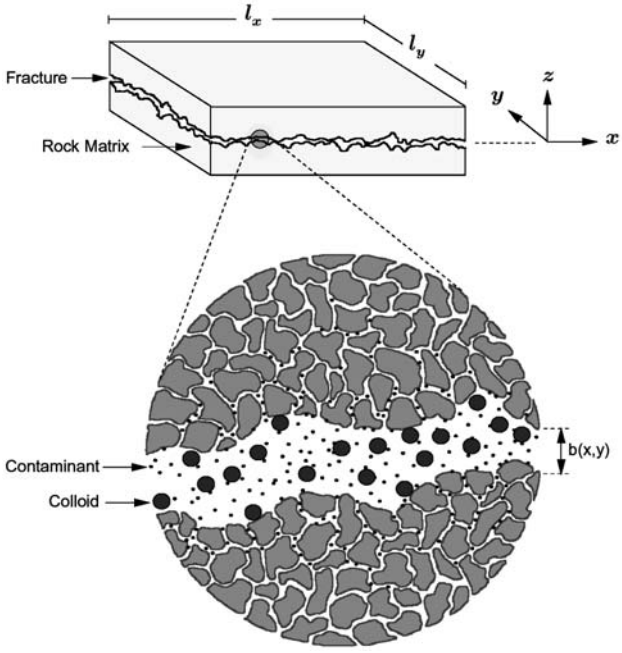

Fig. 1 Schematic illustration of contaminant transport in a quasi-three-dimensional fracture with spatially variable aperture, $b(x,y)$, in the presence of colloids. Contaminants are considered to be molecular (point) size whereas colloids are finitely sized (monodisperse or polydisperse). Contaminants can sorb onto colloids as well as onto the fracture walls and may diffuse into the rock matrix. Colloids attach onto the fracture walls, but do not penetrate the rock matrix. Note that $z=0$ m at the center of the fracture. The model assumes a fracture without fill or gouge

Colloids

Colloids are subject to advection, diffusion, and attachment onto the fracture walls. They may not diffuse into the surrounding porous matrix based on the assumption that the size of a colloid is greater than the pore size of the surrounding matrix (Abdel-Salam and Chrysikopoulos 1995a). Although studies have shown that under certain circumstances colloids may diffuse into the rock matrix (Cumbie and Mckay 1999), in this work, results are presented for colloids that do not penetrate the matrix, which is consistent with most numerical models of co-transport (e.g., Grindrod 1993; Ibaraki and Sudicky 1995a; Baek and Pitt 1996; Baik and Hahn 1997; Jen and Li 2000). In addition, while the numerical model could easily incorporate this phenomenon, neglecting colloid diffusion into the rock matrix represents the type of conservative modeling often used for performance assessment of waste repositories.

Colloids travel by advection in the x- and y-directions according to the local parabolic velocity profiles given by Eqs. 1 and 2, and diffuse isotropically in all directions. The general advective/diffusive particle tracking equations used for colloids are (Tompson and Gelhar 1990; James and Chrysikopoulos 2000):

$$x^{m+1} = x^m + u_x(x^m, y^m, z^m)\Delta t + Z(0,1)\sqrt{2\mathcal{D}_n \Delta t}, \quad (3)$$

$$y^{m+1} = y^m + u_y(x^m, y^m, z^m)\Delta t + Z(0,1)\sqrt{2\mathcal{D}_n \Delta t}, \quad (4)$$

$$z^{m+1} = z^m + Z(0,\ 1)\sqrt{2\mathcal{D}_n \Delta t} \quad (5)$$

where x^{m+1}, y^{m+1}, and z^{m+1} are the colloid's updated coordinates at time $m+1$, Δt is the time step, $Z(0,1)$ is a random selection from the standard normal (Gaussian) distribution, and $\mathcal{D}_n$ is the isotropic diffusion coefficient. The diffusion coefficient for a colloid is calculated from the Stokes–Einstein equation,

$$\mathcal{D}_n = \frac{kT}{3\pi\mu d_p}, \quad (6)$$

where d_p is the colloid diameter, k is Boltzmann's constant, and T is the absolute temperature and μ the kinematic viscosity of the interstitial fluid.

Upon movement between fracture elements with different apertures, a new colloid z-location must be calculated. A ratio valid under creeping flow conditions in slowly converging or diverging channels is used (Haber and Brenner 1993):

$$z_{new} = z_{old}\frac{b_{new}}{b_{old}}. \quad (7)$$

Colloids may travel either perpendicularly or diagonally between elements, however only the initial and final z-locations and apertures are used in Eq. 7.

Contaminants

Contaminants move through the fracture by advection and dispersion in the x- and y-directions and their transport is retarded by sorption onto the fracture walls and diffusion into and sorption onto the surrounding porous rock matrix. Contaminants may sorb onto colloids, thereafter adopting the transport properties of the carrier colloid. The particle tracking equations used for aqueous phase contaminants in the x- and y-directions are:

$$x^{m+1} = x^m + \bar{u}_x(x^m, y^m)\Delta t + Z(0,1)\sqrt{2D_{Taylor}\Delta t}, \quad (8)$$

$$y^{m+1} = y^m + \bar{u}_y(x^m, y^m)\Delta t + Z(0,1)\sqrt{2D_{Taylor}\Delta t}, \quad (9)$$

where D_{Taylor} is the Taylor dispersion coefficient. Taylor dispersion arises from the combination of a velocity gradient and molecular diffusion and is defined as (Taylor 1953; James and Chrysikopoulos 2003b)

$$D_{Taylor} = \mathcal{D}_c + \frac{1}{210}\frac{\bar{u}^2_{x,y}(x,y)b^2(x,y)}{\mathcal{D}_c} \quad (10)$$

where $\mathcal{D}_c$ is the molecular diffusion coefficient of the contaminant, and $\bar{u}_{x,y}(x,y)$ is the local velocity in the x-direction in Eq. 8 or the y-direction in Eq. 9. Note that contaminants are advected according to the average x- and y-velocities rather than by Eqs. 1 and 2. This

method provides an accurate approximation of contaminant movement because for the flow conditions modeled here (Re$\sim$2.3×10^{-3}), a dissolved contaminant rapidly diffuses across flow streamlines (z-direction), adopting local velocities along the way and effectively traveling at the mean fluid velocity within a short time. The validity of using effective parameters (Taylor dispersion) and reducing the model dimension has been demonstrated for transport in a uniform aperture fracture (James and Chrysikopoulos 2003b, Fig. 5).

Description of the colloid and contaminant plumes

A total of 10,000 contaminant and 10,000 colloid particles are released instantaneously ($t=0$ s) across the inlet ($x=0$ m) of the fracture. The colloid plume is assumed to be either monodisperse of size $d_p=5\times10^{-6}$ m, or polydisperse with mean size $\mu_{d_p}=1\times10^{-6}$ m and standard deviation $\sigma_{d_p}=0.9\times10^{-6}$ m.Each colloid is assigned a finite number of contaminant sorption sites and when all sites have been filled, it is no longer available for further reaction with contaminants. The contaminant plume is composed of homogeneous, dissolved, reactive molecules that are modeled as infinitesimal particles. A representative diffusion coefficient, $\mathcal{D}_c=9\times10^{-10}$ m^2/s, was chosen for the contaminants in water at $T=285$ K with $\mu=1.003\times10^{-3}$ kg/m s that equates to a molecule size of 4.7 Å (Welty et al. 2001).

The colloid and contaminant plumes are introduced at the inlet side of the fracture flow domain and distributed according to the local volumetric flow rate. A discrete cumulative probability density function based on the volumetric flow rate into each inlet element of the fracture is constructed by summing all individual element flow rates at the fracture inlet and determining each element's contribution (probability) to the sum. After normalizing this cumulative probability, a uniformly distributed random number between 0 and 1 is generated for each colloid and contaminant. The random number's placement in the cumulative distribution of the flow rates at the inlet designates the corresponding entrance element, j, from the 80 distinct entrance elements. Once the element is specified, $1\le j\le 80$, a particle's exact y-coordinate (in meters) is assigned by the equation:

$$y=\frac{(j-1)+\mathrm{Rn}(0,1)}{20}, \tag{11}$$

where Rn(0, 1) is a uniformly distributed random number between 0 and 1, and j is numbered 1 through 80 in the positive y-direction. Thus, if a particle is assigned a j value of 4, its initial y-location will fall between $y=0.15$ m and $y=0.2$ m. If the random number is Rn(0,1) = 0.24, the particle's initial y-location from Eq. 11 is $y=0.162$ m.

Finally, within an entrance element, the z-location of a colloid perpendicular to the fracture wall must be specified. It is assumed that the probability of a colloid entering a fracture element at a given z-location is proportional to the local flow rate in the corresponding parabolic velocity profile (Reimus 1995; James and Chrysikopoulos 2000). Furthermore, its centroid must be located a distance of at least $d_p/2$ m from the fracture wall to ensure that it is wholly contained within the fracture. Numerically, colloid centroids are selected until this criterion is met.

Time step selection

Both solution accuracy and computational efficiency must be considered when choosing the magnitude of the time step for a particle tracking algorithm. Unfortunately, improving computational efficiency compromises solution accuracy and vice versa. Increased accuracy is achieved by reducing the time step to gain finer resolution of a particle's motion, while computational efficiency is improved by increasing the time step, thereby reducing the number of steps necessary to attain the desired solution. An appropriate balance between these two objectives must be achieved that satisfies each to a reasonable degree. The great disparity in magnitudes of diffusion coefficients for colloids and contaminants complicates the selection of a time step.

It should be noted that diffusive spreading is proportional to $(\Delta t)^{1/2}$ in a particle tracking equation (James and Chrysikopoulos 2001; Reimus and James 2002). A time step of $\Delta t=30$ s is chosen such that a colloid released at $z=0$ m (the center of the fracture) would typically diffuse across only 10% of the average aperture, $\bar{b}$, in a single time step. Unfortunately, this 30 s time step yields a range of diffusion distances for dissolved contaminants that extends far beyond the average fracture aperture. Quantitatively, the mean diffusion distance for contaminants is nearly two orders of magnitude larger than that for colloids due to the three order of magnitude difference between the diffusion coefficients. Because of the prohibitively small time step required for resolution of the contaminants in the z-direction (10^{-2} s), within the fracture they are modeled two-dimensionally, i.e., only the x- and y-movements are tracked. Fortunately, contaminants need not be tracked in the z-direction while flowing in the fracture based on the assumption that an aqueous contaminant plume subject to Taylor dispersion travels with the local average fluid velocity.

Interaction with the fracture surfaces

Colloids

When a colloid encounters a fracture wall, it either reflects back into the fracture or attaches onto the wall. The probability of colloid attachment onto fracture

walls, p_a, may be represented by an equation derived from the Boltzmann law (Adamczyk et al. 1991).

$$p_a = \exp\left(-\frac{\Phi_n}{kT}\right), \tag{12}$$

where Φ is the repulsive energy of interaction between the particle and the fracture surface. A value of $\Phi_n = 10kT$ J is suggested by Adamczyk et al. (1992a, b) as a general approximation assuming low sodium and calcium concentrations (Missana et al. 2003). A value of $\Phi_n \to \infty$ J implies infinite repulsion and no wall deposition. Equation 12 is a simplified representation of the attachment process and other more complex functions could easily be substituted if appropriate site data are available.

To ultimately determine whether a particle will attach onto the wall, a uniformly distributed random number between zero and one is generated each time a wall encounter is recorded and compared to the attachment probability, p_a. If the random number is less than the attachment probability, the colloid attaches onto the wall; otherwise, the particle is reflected back into the fracture. That is, the final x- and y-coordinate positions remain unchanged, whereas the final z-coordinate is set a distance away from the wall equal to the distance that the particle would have obtained had it penetrated the rock matrix, plus the particle diameter. For example, if a particle of $d_p = 5\times10^{-6}$ m is initially estimated to move to a z-location of 5.21×10^{-5} m in one time step (where the fracture wall is located at $x = 5.0\times10^{-5}$ m), its reflected z-location would be 4.29×10^{-5} m.

Contaminants

During each time step, an aqueous contaminant in the fracture has opportunity to diffuse into the matrix or sorb onto the fracture wall. Because the model does not track the motion of contaminants in the fracture in the z-direction, wall encounters cannot be physically counted. Instead, an expression to calculate the probability of a contaminant wall encounter as a function of time van der Lee et al. 1994, Eq. 7):

$$p_c = \frac{\sqrt{\pi \mathcal{D}_c t_e}}{b(x,y)} \operatorname{erf}\left[\frac{b(x,y)}{2\sqrt{\mathcal{D}_c t_e}}\right], \tag{13}$$

where erf() is the error function and t_e is the time when p_c is expected to equal 0.5. During a 30 s time step, the contaminant has ample opportunity to diffuse across the fracture, and typical values for p_c if $t_e = 30$ s are in excess of 0.99 implying that multiple wall encounters are likely each time step. To address this issue, p_c is set equal to 0.5 and Eq. 13 is solved for t_e, which is now the sub-time step that results in a 50% chance of a wall encounter for a contaminant. Dividing Δt by $2t_e$ yields the approximate number of wall encounters expected per time step.

Three options are available to a contaminant each time it encounters the fracture wall. First, the contaminant may diffuse into the porous matrix with probability equal to the porosity,θ. A new uniformly distributed random number is drawn; if it is less than θ, it is assumed that the particle has encountered a pore and it will diffuse a distance of $\sqrt{\mathcal{D}_c t_{\Delta-e}}$m into the matrix during that time step, where $t_{\Delta-e}$ is the remaining time in Δt after the elapsed number of sub-time steps before a pore was encountered has been subtracted. Second, if no pore is encountered, a contaminant may sorb onto the wall according to the Boltzmann law, Eq. 12, with $\Phi_n$replaced with Φ_c. Values of $\Phi_c$used are $15kT$, $14kT$, and $13kT$. Finally, if a contaminant neither diffuses into the porous matrix nor sorbs onto the fracture wall, it continues moving freely within the fracture according to Eqs. 8 and 9.

Contaminant transport in the rock matrix

If a contaminant has successfully diffused into the porous matrix, it is modeled three-dimensionally (i.e., x-, y-, and z-movement is tracked). Due to the abrupt spatial variance at the fracture wall in both the diffusion coefficient and the porosity, two additional deterministic 3-directions velocities are applied to a contaminant within the matrix to avoid the false accumulation of particles in stagnant and/or low porosity zones within the matrix (Reimus 1995, p. 19). These velocities apply only within the transition layer that is within a specified distance from the fracture-wall interface. The transition layer thickness was chosen to be half the average fracture aperture, $\Delta z_{trans} = \bar{b}/2 = 2.5\times10^{-5}$m. Transition zone thickness is difficult to determine experimentally and its best use in the model may be as a fitting parameter. Across the transition layer, the diffusion coefficient and matrix porosity are assumed to vary linearly from their fracture values to their values at the end of the transition layer, $\mathcal{D}$ and 1, to $\theta\mathcal{D}_c$ and θ, respectively. Deterministic velocities are expressed as (Tompson and Gelhar 1990):

$$U_{\mathcal{D}} = (\nabla \mathcal{D}_c) = \mp\frac{2\mathcal{D}_c(\theta - 1)}{\bar{b}}, \tag{14}$$

$$U_\theta = \mathcal{D}_c(\nabla \ln\theta) = \mp\frac{2\mathcal{D}_c \ln\theta}{\bar{b}}, \tag{15}$$

where $U_{\mathcal{D}}$ is the deterministic velocity that compensates for the decrease in diffusivity and $U_\theta$counteracts the abrupt decrease in porosity. These terms, which are positive in the $-z$ direction, serve to move the contaminants out of the porous matrix and back into the fracture.

Thus, the system has two distinct, symmetric regions about the center of the fracture ($z = 0$ m), each governed by a variation of the particle tracking equations. These regions are the fracture void space where contaminants undergo advection and diffusion according to Eqs. 8

and 9; and the porous matrix where contaminant transport is governed by the molecular diffusion coefficient and the matrix porosity only. Recall that a contaminant that has diffused into the matrix is assigned a z coordinate of $z_{\text{matrix}} = \sqrt{\mathcal{D}_c t_{\Delta-e}}$m, where $z_{\text{matrix}} = 0$ m at the fracture-matrix boundary. The contaminant particle tracking equations within the transition layer of the matrix are:

$$x^{m+1} = x^m + Z(0,\,1)\sqrt{2\theta\mathcal{D}_c\Delta t}, \tag{16}$$

$$y^{m+1} = y^m + Z(0,\,1)\sqrt{2\theta\mathcal{D}_c\Delta t}, \tag{17}$$

$$z^{m+1}_{\text{matrix}} = z^m_{\text{matrix}} + Z(0,\,1)\sqrt{2\theta\mathcal{D}_c\Delta t} \pm \frac{2\mathcal{D}_c}{\bar{b}}(\ln\theta + \theta - 1)\Delta t, \tag{18}$$

where the last term in Eq. 18 is due to the deterministic velocities, Eqs. 14 and 15, with the sign opposite to the sign of z. If a contaminant diffuses beyond the transition layer, the last term in Eq. 18 is dropped. In the event that a contaminant diffuses back into the fracture (i.e., its z_{matrix} value becomes negative), its transport is once again governed by Eqs. 8 and 9.

Contaminant sorption onto the matrix

Sorption and desorption of contaminants onto the matrix are handled probabilistically with the intent of modeling a first-order kinetic sorption reaction. Based on the work of Valocchi and Quinodoz (1989 , Eq. 11), two reaction constants are defined: k_f is the forward reaction rate, and k_r is the remobilization rate. The equation

$$t_f = -\frac{1}{k_f}\ln[\text{Rn}(0,\,1)], \tag{19}$$

is used to specify the difference between the time a contaminant penetrates the matrix and the time until it sorbs. Once a contaminant diffuses into the matrix, t_f is calculated, added to the current time, and stored. If the model steps past this time and the contaminant has not exited the matrix, it has sorbed onto the matrix.

A similar equation describes the length of time for which the contaminant is sorbed

$$t_r = -\frac{1}{k_r}\ln[\text{Rn}(0,\,1)], \tag{20}$$

where t_r is the sorption time and k_r is the reverse reaction rate. If k_r is zero, sorption time is infinite and the contaminants are assumed to sorb irreversibly. A uniformly distributed random number is substituted into the preceding equation, a sorption time is calculated, added to the current time, and stored. Once the model steps past this stored time, the contaminant is released from the matrix and is transported according to Eqs. 16, 17 and 18.

Note that equilibrium sorption could alternatively be modeled by dividing the total distance traveled each time step as calculated by Eqs. 16, 17, and 18by a retardation factor.

Contaminant/colloid co-transport

Based on the relatively short travel time in the system modeled here, a first-order kinetic sorption model is used to model the attachment of contaminants onto colloids (Möri et al. 2003). Because the particle tracking model specifies the number of contaminants in each fracture element rather than contaminant mass per volume, the following equation is used:

$$\frac{\partial C^*_f(x,y)}{\partial t} = \frac{K_n}{b(x,y)}C_f(x,y), \tag{21}$$

where $C_f(x, y)$ is the number of aqueous contaminants in a fracture element, $C^*_f(x, y)$ is the integer-rounded number of contaminants that have sorbed onto colloids in a fracture element, and K_n is the first-order partition coefficient, which effectively measures the affinity between the dissolved contaminant and the colloid. Note that the number of contaminants expected to sorb onto colloids in a particular fracture element is inversely proportional to the aperture of that element (i.e., the same number of contaminants in a narrow aperture element compared to a wider aperture element results in greater particle number density, leading to more potential contaminant-colloid collisions, and consequently to an increase in number of contaminants sorbed onto colloids).

The left hand side of Eq. 21 is replaced with $\Delta C^*_f/\Delta t$to determine the maximum increase in the number of co-transported contaminants in each element during a time step:

$$\Delta C^*_f(x,y) = \frac{K_n}{b(x,y)}C_f(x,y)\Delta t. \tag{22}$$

Because the predicted number of contaminant–colloid collisions leading to contaminant sorption onto colloids is limited by the number of available colloid sorption sites in an element, the total number of unoccupied sorption sites must be counted in each element at the conclusion of each time step. In the event that there are no available sorption sites on colloids within an element, the remaining contaminants predicted to undergo sorption onto colloids remain in the aqueous phase. Assuming there are sufficient colloid sorption sites available, an appropriate colloid must be chosen. To preserve spatial continuity, a contaminant can sorb only onto a colloid that is in the same fracture element. If a suitable colloid is found (i.e., one with available sorption sites that is within the same fracture element), the contaminant will sorb onto it and assume its transport properties. The particular colloid chosen for a sorption reaction within the fracture element is arbitrary.

Once an aqueous contaminant sorbs onto a colloid, its new x- and y-locations are updated according to the movement of the carrier colloid. The contaminant is now prevented from diffusing into the porous matrix, and can only associate with the fracture wall if the carrier colloid attaches. The transport properties of the colloid are unaltered by the contaminant sorbed onto its surface. Upon sorption of a contaminant, the number of available sorption sites for that colloid is reduced by one.

Contaminants may also sorb onto colloids that have been deposited on fracture walls. An equation analogous to Eq. 22 is used to predict the change in the number of contaminants sorbed onto deposited colloids using a modified partition coefficient,

$$\Delta C_{\mathrm{f}}^{*}(x,y) = \frac{K_{\mathrm{n}}^{*}}{b(x,y)} C_{\mathrm{f}}(x,y)\Delta t. \tag{23}$$

Similar to contaminant desorption from the matrix, contaminants may desorb from mobile colloids according to Eq. 20 with rate K_{r} and from attached colloids with rate K_{r}^{*}. Because of the relatively short simulation time of these models, the effects of desorption are minute and will be investigated in future modeling efforts.

Model parameters

The modeling of colloid and contaminant transport in a fracture incorporates numerous model parameters. Because of the many variables it was necessary in the present study to limit the sensitivity analysis only to the parameters most likely impact co-transport behavior. For example, scoping model runs indicate that the effect of attached colloids on co-transport processes is negligible for the colloid concentrations studied here, therefore, the reaction parameter, K_n^{*}, is set equal to zero. Furthermore, because the time-frame of these simulations is relatively short, ~35 h, reversible reactions are neglected here, but will be investigated in future work. In addition, reversible reactions have already been presented by Abdel-Salam and Chrysikopoulos (1995a). Constant parameters used in the model simulations presented in this work are listed in Table 1. In general, the parameters used in this work are not intended to apply to any specific physical system. Rather, the intention of this manuscript is to present a model of colloid facilitated contaminant transport and to focus on its utility in any context. The primary goal is to illustrate the model's versatility demonstrating that it could be applied to various co-transport problem scenarios. Parameters were selected to illustrate the model results although they could easily be changed to approximate parameters found at any geologic site. In addition, the model could be run with a code like PEST (Watermark Computing 2002) to estimate reaction parameters by matching breakthrough curves with experimental data.

Numerical simulations and results

Uniform aperture fracture

An analytical solution to both finitely- and point-sized particle conservative (i.e., non-sorbing and zero matrix porosity) transport in a uniform aperture fracture is employed to confirm the accuracy of the particle tracking model for both monodisperse and polydisperse colloids. The time and space dependent colloid or contaminant number concentration is (James and Chrysikopoulos 2003a),

$$\bar{n}(x,t) = \frac{n_{\mathrm{o}}}{(4\pi D_{\mathrm{eff}} t)^{1/2}} \exp\left[-\frac{(x-U_{\mathrm{eff}}t)^2}{4D_{\mathrm{eff}}t}\right], \tag{24}$$

where n_0 is the initial particle number concentration and U_{eff} and D_{eff} are the effective velocity and dispersion coefficients defined as (James and Chrysikopoulos 2003b):

$$U_{\mathrm{eff}} = \bar{u}_x\left[1 + \frac{d_{\mathrm{p}}}{b} - \frac{1}{2}\left(\frac{d_{\mathrm{p}}}{b}\right)^2\right], \tag{25}$$

and

$$D_{\mathrm{eff}} = \mathcal{D}_{\mathrm{n}} + \frac{1}{210}\frac{\bar{u}_x^2 b^2}{\mathcal{D}_{\mathrm{n}}}\left(1 - \frac{d_{\mathrm{p}}}{b}\right)^6, \tag{26}$$

where $\bar{u}_x$ is the average interstitial velocity of the parabolic velocity profile in the uniform aperture fracture. For infinitesimally small contaminants, $d_{\mathrm{p}} = 0$, reducing Eq. 25 to the mean fluid velocity and Eq. 26 to the Taylor dispersion coefficient.

Assume that the uniform aperture fracture with aperture, $b = 5\times 10^{-5}$ m, is water saturated and 8 m long. Within the fracture, water flows with average interstitial velocity $\bar{u}_x = 6\times 10^{-5}$ m/s and the matrix is non-porous (no matrix diffusion, $\theta = 0$). Figure 2 shows both analytical (solid curves) and numerical (dashed curves) breakthrough curves for the monodisperse (M) and polydisperse (P) colloid and contaminant (C) plumes. Excellent agreement is shown between the two solutions for both colloids and contaminants demonstrating the accuracy of the particle tracking model. Furthermore, the similarity between the contaminant particle tracking solution and the analytical solution supports the assertion that two-dimensional treatment of the contaminant plume is appropriate.

In the uniform aperture fracture, it is assumed that advection and molecular diffusion or Taylor dispersion of the plumes are the only parameters influencing particle transport. The average elution times (time for 50% breakthrough) are 33.8 h for the monodisperse colloid plume, 36.5 h for the polydisperse plume, and 37.0 h for the contaminant plume, corresponding to effective velocities of 6.57×10^{-5}, 6.09×10^{-5}, and 6.0×10^{-5} m/s, respectively. Note that the effective velocity of the col-

Table 1 Constant model parameters and values

Parameter	Value
$\bar{b}$	5×10^{-5}m
d_p	5×10^{-6} m
$\mathcal{D}_c$	9×10^{-10} m^2/s
k	1.38×10^{-23} J/kg K
k_r	0 s^{-1}
K_n^*	0 m/s
K_r	0 s^{-1}
K_r^*	0 s^{-1}
ℓ_x	8 m
ℓ_y	4 m
T	288 K
Δt	30 s
Δx, Δy	0.05 m
μ	1.003×10^{-3} kg m/s
μ_{d_p}	1×10^{-6} m
σ_{d_p}	0.9×10^{-6} m

loid plume is consistent with Eq. 25, which also yields a velocity of 6.57×10^{-5} m/s for colloids with $d_p = 5\times10^{-6}$ m, while contaminants move with the average fluid velocity, $\bar{u}_x = 6.0\times10^{-5}$m/s. Furthermore, using the median colloid size of the polydisperse plume (0.72 μm) in Eq. 25 yields an effective velocity of 6.09×10^{-5} m/s. Note the difference between the slopes of the breakthrough curves in Fig. 2. The contaminant breakthrough curve is significantly steeper than the colloid curve, indicating less axial spreading of the contaminant plume and providing further verification that dissolved contaminants travel with the mean fluid velocity. According to Eqs. 26 and 10, the dispersion coefficients of the monodisperse colloids and contaminants are 2.71×10^{-7} m^2/s and 9.48×10^{-10} m^2/s, respectively. The Taylor dispersion coefficient of the contaminant plume is only slightly larger than its molecular diffusion coefficient, while the dispersion coefficient of the monodisperse colloid plume is six orders of magnitude larger than its diffusion coefficient.

Variable aperture fracture

In the following figures, colloids are represented with solid lines and contaminants with dashed lines unless otherwise noted. Additionally, all breakthrough curves are the ensemble average of 100 variable aperture fracture realizations. Figure 3 shows breakthrough curves of nonreacting plumes, monodisperse (M) and polydisperse (P) colloids and contaminants (C), traveling through a variable aperture fracture under the influence of advection, diffusion, and dispersion. Sorption onto the fracture surfaces and diffusion into the rock matrix are not allowed. In a variable aperture fracture, water flows preferentially along the least resistive pathway where the fracture elements are widest. The tortuosity of these preferential pathways, combined with transverse molecular diffusion across streamlines leads to the observed mechanical dispersion.

All three breakthrough curves exhibit increased spreading and tailing when compared to curves from the uniform aperture fracture in Fig. 2 (note the difference in time scale on the x-axis). In contrast to the breakthrough curves from a uniform aperture fracture, the slopes of these curves are similar, indicating that mechanical dispersion in a variable aperture fracture is the dominant spreading mechanism. Note also that the colloid plume again exits the fracture ahead of the contaminant plume. The enhanced transport of the plume, as previously discussed, is the result of colloid size exclusion from the slowest moving portion of the velocity profile neareast the wall.

Colloid Wall Deposition

The colloid wall deposition parameter, Φ_n, was varied for a set of simulations to examine only the effect of deposition onto fracture wall surfaces (no matrix diffusion) on the normalized fraction of colloids exiting the fracture. Figure 4a and b illustrate the model simulations for monodisperse and polydisperse colloids, respectively. Polydisperse colloids are more sensitive to variations in Φ_n than are the monodisperse colloids. Because of the larger diffusion coefficients for the small members of the polydisperse colloid plume, these colloids have more frequent encounters with the fracture walls and therefore more opportunity to attach onto the fracture walls compared to the larger colloids. As expected, decreasing the value of Φ_n, thereby increasing the sorption probability, results in a decreased fraction of colloids eluted.

Contaminant matrix diffusion and wall deposition

When contaminants diffuse into the matrix, significant retardation of the plume occurs, as seen in Fig. 5a. As the contaminant plume passes through the fracture, the

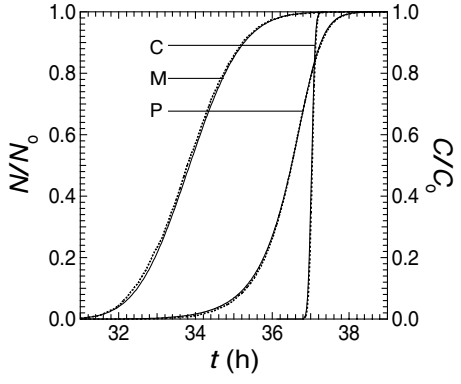

Fig. 2 Monodisperse M, ($d_p = 5\times10^{-6}$ m) and polydisperse P, ($\mu_{d_p} = 1\times10^{-6}$ m, $\sigma_{d_p} = 0.9\times10^{-6}$ m) colloid and contaminant C, analytical (*solid curves*) and numerical (*dashed curves*) breakthrough curves at $x = 8$ m in a uniform aperture fracture with $b = 5\times10^{-5}$ m and $\bar{u}_x = 6\times10^{-5}$ m/s. Here, $\Phi_n = \infty$, $\theta = 0$, and $k_f = k_r = K_n = K_r = K_n^* = K_r^* = 0$

sharp concentration gradient between the fracture and the rock matrix drives contaminants into the rock matrix. As the bulk of the contaminant plume continues through the fracture, the direction of the concentration gradient reverses. When the contaminant concentration inside the fracture decreases in the wake of the contaminant plume, contaminants emerge from the matrix and resume their transport down the fracture. As expected, this results in contaminant retardation because contaminants that enter and subsequently exit the matrix exhibit significantly increased residence times. In the absence of contaminant sorption onto the structure of the rock matrix, nearly all of the contaminants ultimately diffuse back into the fracture. Because the number of contaminants that diffuse into the matrix is an increasing function of the porosity, greater porosity results in more retardation. While not visually evident, it should be noted that the arrival time of the first colloids in all plumes in Fig. 5a is at ~30 h. Although Neretnieks (1980) presents a constant source analytical solution to transport in a fracture with diffusion into the matrix, it is not of comparable form to the work presented here (instantaneous injection).

Figure 5b illustrates the effects of decreasing interaction energy between contaminants and non-porous fracture walls. Contaminants irreversibly sorb onto the fracture walls as the interaction energy decreases and remain in the system in increasing numbers. It is not surprising that even for a smaller interaction energy, a contaminant plume demonstrates increased reaction with the fracture wall compared to a colloid plume because the contaminants exhibit a significantly larger number of wall encounters.

Fracture wall deposition and matrix diffusion with sorption

The combined effects of matrix diffusion and wall and matrix sorption processes are illustrated in Fig. 6. A reference curve (no wall deposition or matrix diffusion) is included for comparison to the combined wall deposition and matrix diffusion model simulations. Note the significant retardation experienced by a plume resulting from the combination of matrix diffusion and deposition with $k_f = 1\times10^{-5}$ s^{-1}. Comparison with the corresponding curve in Fig. 4, which has no matrix diffusion, illustrates that significantly fewer contaminants are eluted for the same value of Φ_c when matrix diffusion is considered. The simulated contaminant plume retardation is attributed to contaminants that have diffused into and subsequently sorbed onto the fracture matrix. In the interest of brevity, desorption is not considered in this model, therefore $k_r = 0$.

Co-transport effects

In Fig. 7, snapshots of the discrete x- and y-locations of the infinitesimal particles comprising the contaminant plume undergoing advection, diffusion/dispersion, and co-transport processes in the presence of monodisperse colloids at progressively increasing simulation times are shown. No matrix diffusion, sorption, or attachment onto the rock matrix are simulated. Co-transporting contaminants are represented by open circles and contaminants dissolved in the aqueous phase by closed tri-

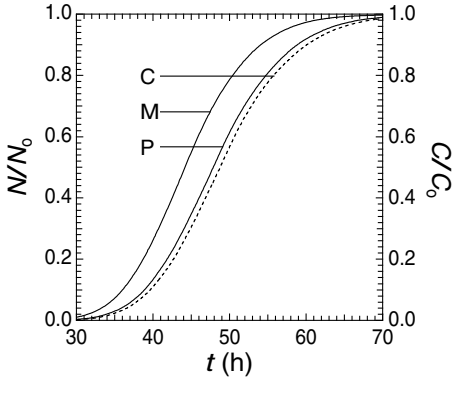

Fig. 3 Ensemble averaged monodisperse M, and polydisperse P, colloid (*solid curves*) and contaminant C, (*dotted curves*) breakthrough curves in a variable aperture fracture with $\overline{b} = 5\times10^{-5}$ m, $\sigma^2_{\ln b} = 0.15$, and correlation length 1 m. Here, $\Phi_n = \infty$, $\theta = 0$, and $k_f^b = k_r = K_n = K_r = K_n^* = K_r^* = 0$

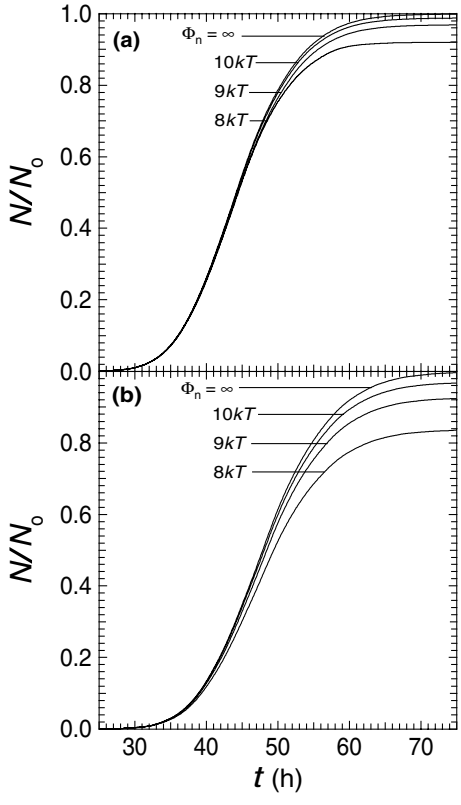

Fig. 4 Ensemble averaged (**a**) monodisperse and (**b**) polydisperse colloid breakthrough curves for a variable aperture fracture subject to several values of the colloid wall deposition parameter, Φ_n. Here, $k_f = k_r = K_n = K_r = K_n^* = K_r^* = 0$

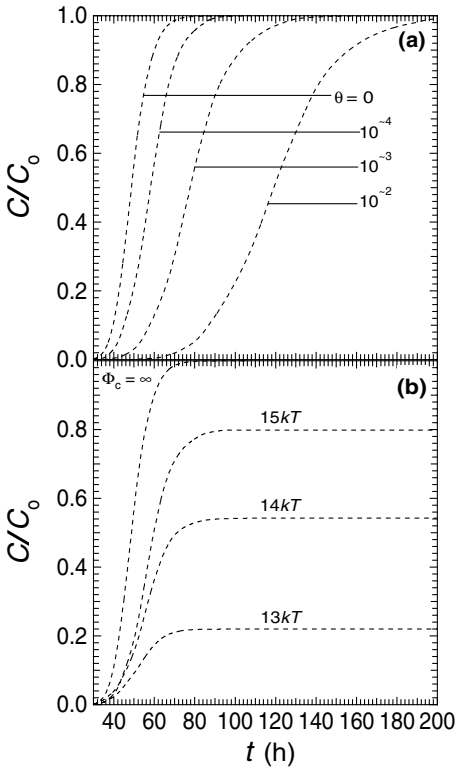

Fig. 5 Contaminant breakthrough curves illustrating the retardation effect of (**a**) matrix diffusion and (**b**) fracture wall deposition ($\theta = 0$). Here, $k_f = k_r = K_n = K_r = K_n^* = K_r^* = 0$

angles. The contaminants that are sorbed onto colloids lead the plume because of the faster average velocity of colloids due to size exclusion. In essence, this shows the contrast between transport with and without colloids as the aqueous contaminants are, so far, unaffected by the presence of colloids and they are shown to trail those contaminants associated with colloids. Again, to limit the scope of this study, contaminants irreversibly sorb onto colloids and $K_r = 0$.

Figure 8 illustrates normalized monodisperse (a–d) and polydisperse (e–h) colloid and contaminant plume breakthrough curves accounting for contaminant matrix diffusion and sorption, wall sorption, and single site-per-colloid co-transport processes in a variable aperture fracture. Horizontally adjacent plots compare normalized breakthrough of monodisperse and polydisperse colloids for identical porosities (θ), interaction energies (Φ_c, Φ_n), and contaminant matrix sorption rates (k_f). Interaction energies decrease, and porosities increase downward between graphs. The contaminant-colloid partition coefficient, K_n, significantly affects the transport of contaminants sorbing onto monodisperse colloids as shown in Fig. 8a and onto polydisperse colloids in Fig. 8e. The breakthrough curves displayed as solid curves correspond to the colloid plume, the last curve (furthest right) corresponds to a non-reacting contaminant plume with $K_n = 0$. As K_n is increased, more contaminants undergo sorption onto the colloids, and the contaminant breakthrough curve collapse onto the colloid breakthrough curve. Contaminant breakthrough is slightly faster in the presence of monodisperse colloids than the polydisperse colloids because the monodisperse colloid size is larger than the average polydisperse colloid size. While colloid curves are not significantly retarded by decreasing Φ_n, contaminant plumes are significantly retarded by a decrease in Φ_c (see also Fig. 5). However, when K_n is increased, more contaminants sorb onto colloids making less available to diffuse into the matrix or sorb onto fracture walls, even if Φ_c is relatively low. Because colloids cannot diffuse into the porous matrix, and in these simulations rarely attach onto the fracture walls, co-transporting contaminants often remain mobile by sorbing onto mobile colloids. Clearly, the presence of co-transport mechanisms decreases the retardation effects otherwise experienced by a contaminant plume. The result is faster transport and increased spreading of the contaminant plume (especially for polydisperse colloid co-transport), and an increase in the normalized percentage of contaminants that are eluted from the fracture. Although such simulations are not presented here, it is conceivable that very low Φ_n and high K_n and K^*_nmay serve to decrease contaminant mobility because contaminants sorb onto colloids that are attached to the fracture wall.

Simulations were performed for colloids with 2.3 sorption sites/nm^2 as suggested by Davis and Kent (1990), however they are not presented here because little difference in the shape of the model breakthrough curves was observed. Increasing the number of particles in each plume may increase the effect of multiple sorption sites, but computational limitations restricted the number of particles in the plumes.

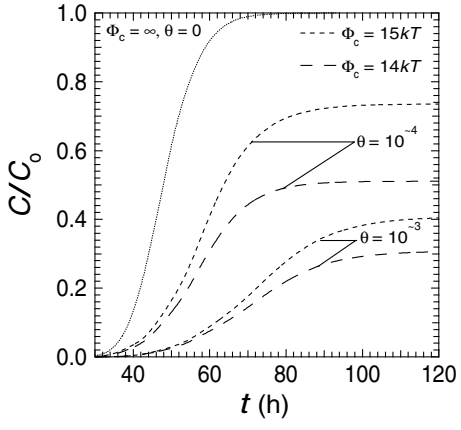

Fig. 6 Contaminant breakthrough curves illustrating the combined effect of fracture wall deposition and matrix diffusion with sorption. Two contaminant wall interaction energies are shown, $\Phi_c = 15kT$ (*short dashed curves*), and $\Phi_c = 14kT$ (*long dashed curves*). A contaminant curve unaffected by deposition flowing through a non-porous matrix is shown for reference (*dotted curves*). Here, $k_f = 1\times10^{-5}$ s^{-1}and $k_r = K_n = K_r = K_n^* = K_r^* = 0$. It should be noted that all contaminants were deposited, i.e., zero breakthrough, when $\theta = 10^{-2}$

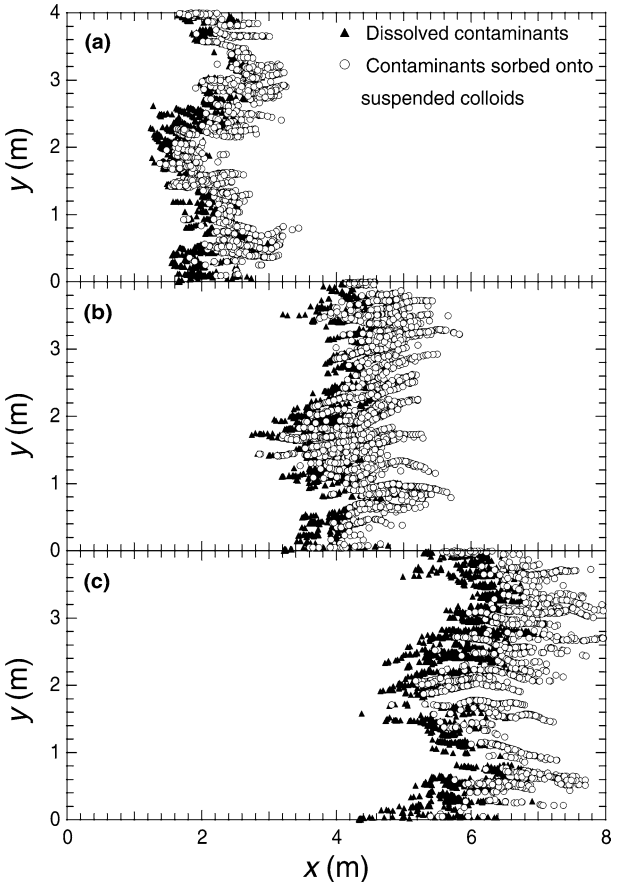

Fig. 7 Snapshots of a contaminant plume traveling through a variable aperture fracture undergoing advection, diffusion, and co-transport processes after (**a**) 40,000, (**b**) 80,000, and (**c**) 120,000 s of simulation. Here, $\Phi_n = \Phi_c = \infty$, $K_n = 1\times\ 10^{-8}$ m/s, and $k_f = k_r = K^*_n = K_r = K_r^* = 0$

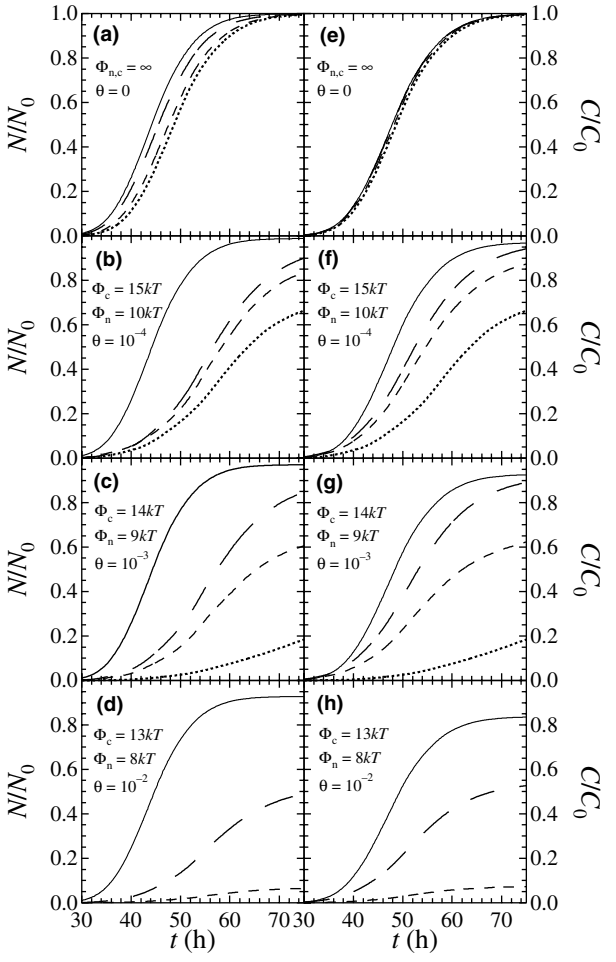

Fig. 8 **a**–**d** Monodisperse M, and **e**–**h** polydisperse P, colloid (*solid curves*) and contaminant (*dotted curves*) breakthrough curves resulting from inclusion of matrix diffusion, sorption, and co-transport processes in a variable aperture fracture. The first-order rate partition coefficient for co-transport are $K_n = 1\times 10^{-8}$ m/s (*short dashed*) and 1×10^{-7} m/s (*long dashed*) yielding increased breakthrough. Colloids have one sorption site per particle, the wall deposition parameter and matrix porosity vary as indicated, and the contaminant/matrix sorption rate is $\mathcal{K}_f = 1 \times 10^{-5}\ \mathrm{s}^{-1}\ \mathrm{s}^{-1}$. Here, $k_r = K_r = K_r^* = 0$

Conclusions

A quasi-three-dimensional particle tracking model is used to investigate the effects of matrix diffusion, wall deposition, and co-transport on the transport properties of plumes of contaminants and colloids flowing through a variable aperture fracture subject to advective, diffusive, and reactive mass transfer. By analyzing the shape of ensemble-averaged breakthrough curves that relate the cumulative normalized number of particles eluted as a function of residence time, it is shown that matrix diffusion and wall sorption processes serve to retard the transport of a contaminant plume, while co-transport enhances contaminant mobility. Matrix diffusion and sorption and fracture wall sorption decrease the number of contaminants eluted from the fracture. However, colloids are too large to diffuse into the matrix and, subject to reasonable wall interaction energies, attach to the wall much less frequently than contaminants. Therefore, co-transport effects become increasingly important when contaminants are able to diffuse into and sorb onto the fracture matrix because the retarding effect of these mechanisms is greatly diminished when a contaminant is associated with a colloid. Finally, when co-transport effects are taken into account, polydisperse colloids increase contaminant spreading compared to monodisperse colloids because of their wider range of velocities and diffusion coefficients.

Acknowledgments This work was partially sponsored by Sandia National Laboratories, a multiprogram laboratory operated by Sandia Corporation, a Lockheed Martin Company, for the United States Department of Energy's National Nuclear Security Administration under contract DE-AC04-94AL85000.

References

Abdel-Salam A, Chrysikopoulos CV (1995a) Analysis of a model for contaminant transport in fractured media in the presence of colloids. J Hydrol 165:261–281

Abdel-Salam A, Chrysikopoulos CV (1995b) Modeling of colloid and colloid-facilitated contaminant transport in a two-dimensional fracture with spatially variable aperture. Transp Porous Media 20(3):197–221

Adamczyk Z, Siwek B, Zembala M (1991) Kinetics of localized adsorption of particles on homogeneous surfaces. J Colloid Interface Sci 151(2):351–367

Adamczyk Z, Siwek B, Zembala M (1992a) Reversible and irreversible adsorption of particles on homogeneous surfaces. Colloids Surf A Physicochem Eng Aspects 62:119–130

Adamczyk Z, Siwek B, Zembala M, Weroński P (1992b) Kinetics of localized adsorption of colloid particles. Langmuir 8:2605–2610

Auset M, Keller AA (2004) Pore-scale processes that control dispersion of colloids in saturated porous media. Water Resour Res 40, w03503. DOI 10.1029/2003WR002800.

Baek I, Pitt WW (1996) Colloid-facilitated radionuclide transport in fractured rock. Waste Management 16(4):313–325

Baik MH, Hahn PS (1997) Radionuclide transport facilitated by polydispersed pseudo-colloids in the fractured rock media. J Nucl Sci Technol 34(1):41–49

Bekhit H, Hassan AE (2005) Stochastic modeling of colloid-contaminant transport in physically and geochemically heterogeneous porous media. Water Resour Res (in press)

Champ DR, Schroeter J (1988) Bacterial transport in fractured rock: a field-scale tracer test at the chalk river nuclear laboratories. Water Sci Technol 20(11/12):81–87

Chrysikopoulos CV, Abdel-Salam A (1997) Modeling colloid transport and deposition in saturated fractures. Colloids Surf A: Physicochem Eng Aspects 121:189–202

Chrysikopoulos CV, James SC (2003) Transport of neutrally buoyant and dense variably sized colloids in a two-dimensional fracture with anisotropic aperture. Transp Porous Media 51(2):191–210

Cumbie DH, McKay LD (1999) Influence of diameter on particle transport in a fractured shale saprolite. J Contam Hydrol 37(1–2):139–157

Cvetkovic V (2000) Colloid facilitated transport by steady random ground-water flow. Phys Fluids 12(9):2279–2294

Davis JA, Kent DB (1990) Surface complexation modeling in aqueous geochemistry. In: Mineral-water interface geochemistry. Mineralogical Society of America, Chap. 5. pp 177–260

Derjaguin BV (1934) Untersuchungen über die reibung und adhäsion. Kolloid Zh 69:155–164

Drever JI (1985) The chemistry of weathering. Reidel, Dordrecht

Grindrod P (1993) The impact of colloids on the migration and dispersal of radionuclides within fractured rock. J Contam Hydrol 13:167–181

Gutjahr AL (1989) Fast fourier transform for random field generation. Project report for los alamos grant, contract 4-r58-2690r. New Mexico Institute of Mining and Technology, Socorro

Haber S, Brenner H (1993) Effect of entrained colloidal particles in enhancing the transport of adsorbable chemical contaminants. J Colloid Interface Sci 155:226–246

Hassan AE, Mohamed M (2003) On using the random walk particle tracking method to simulate transport in single-continuum and dual continua porous media: a comparative study. J Hydrol 275:242–260

Hinsby K, McKay LD, Jorgensen P, Lenczewski M, Gerba CP (1996) Fracture aperture measurements and migration of solutes, viruses, and immiscible creosote in a column of clay-rich till. Ground Water 34:1067–1075

Ibaraki M, Sudicky EA (1995a) Colloid-facilitated contaminant transport in discretely fractured porous media 1. numerical formulation and sensitivity analysis. Water Resour Res 31(12):2945–2960

Ibaraki M, Sudicky EA (1995b) Colloid-facilitated contaminant transport in discretely fractured porous media 2. fracture network examples. Water Resour Res 31(12):2961–2969

James SC, Chrysikopoulos CV (2000) Transport of polydisperse colloids in a saturated fracture with spatially variable aperture. Water Resour Res 36(6):1457–1465

James SC, Chrysikopoulos CV (2001) An efficient particle tracking equation with a specified spatial step for the solution of the diffusion equation. Chem Eng Sci 56(23):6535–6543

James SC, Chrysikopoulos CV (2003a) Analytical solutions for the transport of monodisperse and polydisperse particle suspensions in a uniform fracture. Colloids Surf A: Physicochem Eng Aspects 226:101–118

James SC, Chrysikopoulos CV (2003b) Effective velocity and effective dispersion coefficient for finitely sized particles flowing in a uniform fracture. J Colloid Interface Sci 263(1):288–295

Jen C-P, Li S-H (2000) Effects of hydrodynamic chromatography on colloid-facilitated migration of radionuclides in the fractured rock. Waste Manage 21:499–509

Johns RA, Steade JS, Costanier LM, Roberts PV (1993) Nondestructive measurements of fracture aperture in crystalline rock cores using X-ray computed tomography. J Geophys Res 98(B2):1889–1900

Keller AA (1998) High resolution non-destructive measurement and characterization of fracture apertures. Int J Rock Mech Min Sci 35(8):1037–1050

Keller AA, Sirivithayapakorn S, Chrysikopoulos CV (2004) Early breakthrough of colloids and bacteriophage ms2 in a water-saturated sand column. Water Resour. Res. 40 (W08304). DOI 10.1029/2003WR002676

Kersting AB, Efurd DW, Finnegan DL, Rokop DJ, Smith DK, Thompson JL (1999) Migration of plutonium in groundwater at the nevada test site. Nature 397:56–59

van der Lee J, Ledoux E, de Marsily G (1994) Microscopic description of colloid transport in fractured or porous media. In: Dracos, Stauffer (eds) Transport and reactive processes in aquifers. Balkema, pp 349–355

Marseguerra M, Patelli E, Zio E (2001a) Groundwater contaminant transport in the presence of colloids I: a stochastic non-linear model and parameter identification. Ann Nucl Energy 28:777–803

Marseguerra M, Patelli E, Zio E (2001b) Groundwater contaminant transport in the presence of colloids I: sensitivity and uncertainty analysis on literature case studies. Ann Nucl Energy 28:1799–1807

McKay LD, Gillham RW, Cherry JA (1993) Field experiments in fractured clay till: 2. solute and colloid transport. Water Resour Res 20:1149–1162

Missana T, Mingarro M, Gutierrez MG, Alonso U, Geckeis H, Schaefer T, Rabung T, Vejmelka P, Marquardt C, Ota K (2003) Gts phase V CRR experiment. Technical Report, Rep. NTB 03-02. NAGRA, Baden, p 100

Möri A, Alexander WR, Geckeis H, Geyer F, Eikenberg J, Fierz T, Degueldre C, Missana T (2003) The colloid and radionuclide retardation experiment at the grimsel test site: influence of bentonite on the radionuclide migration in a fractured rock. Colloids Surf A Physicochem Eng Aspects 217(1–3):33–47

Nelson DM, Orlandini KA (1986) Environmental research division progress report 1984-85. Technical Report, Anl-86-15. Argonne National Laboratory

Neretnieks I (1980) Diffusion in the rock matrix: an important factor in radionuclide migration? J Geophys Res 85(B8):4379–4397

Ouyang Y, Shinde D, Mansell RS, Harris W (1996) Colloid-enhanced transport of chemicals in subsurface environments—a review. Environ Sci Technol 26(2):189–204

Pang L, Close M (1999) A field study of nonequilibrium and facilitated transport of Cd in an alluvial gravel aquifer. Ground Water 37(5):785–792

Reimus PW (1995) The use of synthetic colloids in tracer transport experiments in saturated rock fractures. PhD Thesis, Los Alamos National Laboratory, LA-13004-T

Reimus PW, James SC (2002) Determining the random time step in a constant spatial step particle tracking algorithm. Chem Eng Sci 57(21):4429–4434

Reimus PW, Robinson BA, Glass RJ (1993) Aperture characteristics, saturated fluid-flow, and tracer-transport calculations for a natural fracture. In: High-level radioactive waste management. pp 2009–2016

Sirivithayapakorn S, Keller AA (2003) Transport of colloids in saturated media: a pore-scale observation of the size exclusion effect and colloid acceleration. Water Resour Res 39(4):1109. DOI 10.1029/2002WR001583

Smith PA, Degueldre C (1993) Colloid-facilitated transport of radionuclides through fractured media. J Contam Hydrol 13:143–166

Smith PA, Alexander WR, Kickmaier W, Ota K, Frieg B, McKinley IG (2001) Development and testing of radionuclide transport models for fractured rock: examples from the Nagra/JNC radionuclide migration program in the Grimsel test site, Switzerland. J Contam Hydrol 47:335–349

Stumm W (1977) Chemical interaction in particle separation. Environ Sci Technol 11:1066–1070

Taylor GI (1953) Dispersion of soluble matter in solvent flowing slowly through a tube. Proc R Soc London A 219:186–203

Tompson AFB, Gelhar LW (1990) Numerical simulation of solute transport in three-dimensional, randomly heterogeneous porous media. Water Resour Res 26(10):2541–2562

Toran L, Palumbo AV (1992) Colloid transport through fractured and unfractured laboratory sand columns. J Contam Hydrol 9:289–303

Valocchi AJ, Quinodoz HAM (1989) Application of the random walk method to simulate the transport of kinetically adsorbing solutes. In: Proceeding of the symposium held during the third IAHS scientific assembly (Groundwater Contamination. No. 185). pp 35–42

van de Ven TGM (1989) Colloidal hydrodynamics. Academic, London

Verwey EJW, Overbeek JTG (1948) Theory and stability of lyophobic colloids. Elsevier, Amsterdam-Ner York

Vilks P, Baik M-H (2001) Laboratory migration experiments with radionuclides and natural colloids in a granite fracture. J Contam Hydrol 47:197–210

Vilks P, Frost LH, Bachinski DB (1996) Field-scale colloid migration experiments in a granite fracture. J Contam Hydrol 26:203–214

Watermark Computing 2002. Model independent parameter estimation: PEST. User's manual

Welty JR, Wicks CE, Wilson RE (2001) Fundamentals of momentum, heat, and mass transfer, 4th edn. Wiley